13.1 SURFACE OBSERVATIONS WITHIN THE FORWARD-FLANK DOWNDRAFT OF A TORNADIC AND NONTORNADIC SUPERCELL

CHRISTOPHER J. SHABBOTT* AND PAUL MARKOWSKI

Department of Meteorology, Pennsylvania State University, University Park, PA

1. Introduction

For more than two decades, the supercell conceptual model presented by Lemon and Doswell (1979) has remained relatively unaltered in terms of its main features. Two of these main features are regions of downdraft: one on the rear flank of the storm and one on the forward flank. Many past studies (see Markowski 2002 for a review) have directed considerable attention to the rear-flank downdraft (RFD), the development or intensification of which has been closely associated with tornadogenesis in many cases. Of interest in this paper is the forward-flank downdraft (FFD), which forms downwind (with respect to the midlevel, storm-relative flow) of the updraft as condensate produced in the updraft is advected downstream. As the precipitation falls into subsaturated air, latent chilling leads to the formation of the FFD. Precipitation loading also contributes to the negative buoyancy within the FFD. The negatively buoyant air descends to the surface and a gust front separates the relatively cool FFD outflow from the warm environmental inflow.

The potential importance of the FFD in supercell dynamics became recognized in numerically simulated studies, which showed that baroclinic generation of horizontal vorticity along the forward-flank gust front can be tilted into the vertical and stretched, providing a source of low-level vertical vorticity and low-level mesocyclone rotation (Klemp and Rotunno 1983; Rotunno and Klemp 1985; Davies-Jones and Brooks 1993). A significant streamwise vorticity component can be aquired since the storm-relative flow often is nearly parallel to the isentropes along the forward-flank gust front. In Klemp and Rotunno's (1983, hereafter KR83) simulation, horizontal vorticity created along the FFD gust front via baroclinic generation was the same magnitude as the environmental horizontal vorticity and was also oriented to produce cyclonic vertical vorticity once tilted. A higher resolution simulation by Wicker and Wilhelmson (1995), in which a tornado-scale vortex could be marginally resolved, corroborated KR83's conclusions regarding the role of the FFD. Rotunno and Klemp (1985) provide further evidence to support their conclusion that baroclinic generation of horizontal vorticity cannot be ignored; in their simulation without precipitation there was no low-level cold pool, and therefore, no low-level mesocyclone.

On the other hand, idealized simulations by Walko

(1993) led one to question the notion that low-level rotation requires the presence of the evaporatively chilled FFD air. His results showed that low-level rotation could be generated by tilting of strong low-to-midlevel *environmental* vorticity, with solenoidal generation producing horizontal vorticity actually having an unfavorable orientation. A downdraft was important in the tilting of vorticity into the vertical in the production of low-level rotation, but not by way of baroclinic processes.

Thermodynamic observations within FFDs have been relatively rare. Indirect observations obtained through buoyancy retrievals by Brandes (1984) might lead some to question whether the role of the FFD is the same in all supercells. Streamwise horizontal vorticity was produced in the Del City-Edmond storm of 20 May 1977, while in the Harrah storm of 8 June 1974, the temperature gradient was reversed, producing an unfavorable orientation of generated horizontal vorticity. Regardless of whether or not the FFD and associated temperature gradient contributes positively to the low-level circulation, at least some baroclinicity is present in the majority of supercells, given the nearly ubiquitous presence of precipitation on the forward flank.

Direct surface thermodynamic observations within FFDs also have been hard to come by. The relatively rare passages of supercells over fixed observing systems combined with the possible hazards of acquiring observations using mobile observation systems makes it difficult to gather dense observations within the FFD. Only a handful of direct measurements have been obtained within FFDs, most of which are limited in spatial coverage. For example, the Arcadia, Oklahoma storm on 17 May 1981 passed over a 444-m-tall instrumented tower (Dowell and Bluestein 1997). A gradual 5°C temperature drop was observed at the surface over a one hour period hinting that the temperature gradient within the FFD was spread over a broad region. However, the tower data do not permit an assessment of the spatial variability of buoyancy within the FFD.

The goal of our ongoing research is to further document the surface conditions within FFDs. Although numerical simulations have indicated an important role for the FFD, we agree with Wakimoto (2001) who states: "detailed observations of the forward-flank downdraft and gust front are still lacking. These analyses would be useful complements to the high-resolution numerical simulations presented in the literature (i.e., Klemp 1987; Wicker and Wilhelmson 1995)." Observations have barely scratched the surface with regards to capturing the range of thermodynamic properties within

* *Corresponding author address*: Mr. Christopher Shabbott, Department of Meteorology, Pennsylvania State University, 503 Walker Building, University Park, PA 16802; *e-mail*: shabbs@psu.edu.
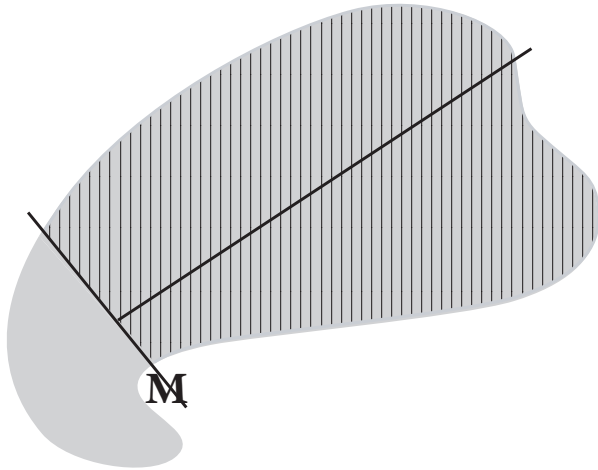
FIG. 1. Schematic of a supercell with radar reflectivity factor shaded. The vertical lines indicate the forward flank. The FFD was defined as the region of reflectivity on the forward side of the line drawn orthogonal to the major axis of the echo through the radar observed circulation center.

FFDs, their relationship to storm evolution and their association with the large-scale environment. Our current research relies on surface data collected by a mobile mesonet within supercell thunderstorms during the 1994–1999 period. The capabilities of this obseving system have been demonstrated in serveral past studies (e.g., Rasmussen et al. 1996; Markowski et al. 2002).

A description of data and analysis methods appears in section 2. This is followed by a summary of the analysis we have completed to date, which includes one tornadic and one nontornadic case (section 3). Section 4 contains a summary and some closing remarks.

2. Data and analysis methods

Analyses of mobile mesonet data obtained within the FFDs of two supercells are presented from two cases: 16 May 1995 and 20 May 1998. The 16 May 1995 case featured a well-documented (Wakimoto et al. 1998; Wakimoto and Liu 1998) tornadic supercell during the Verification of the Origins of Rotation in Tornadoes Experiement (VORTEX; Rasmussen et al. 1994). The 20 May 1998 case provided data in a nontornadic supercell which was observed during a smaller, post-VORTEX field experiment. For both cases, all times in which data were available were examined in order to determine which times had the best spatial coverage and observation density within the FFD region.

The shape and size of precipitation fields associated with supercells often vary by storm, so there was a need to objectively define the FFD region of a supercell. The FFD was defined as *the region of reflectivity on the forward side of the line drawn orthogonal to the major axis of the echo through the radar observed circulation center* (Fig. 1). Although no attempt to objectively define the FFD is free of limitations, the consistent application of a single definition from case to case allows for meaningful comparisions of FFDs to be made. The mobile mesonet data were recorded at 2-s intervals. The

variables recorded were time, latitude, longitude, temperature, relative humidity, pressure, and wind velocity. Virtual potential temperature, θ_v, and equivalent potential temperature, θ_e, are analyzed herein. Calculations of θ_v incorporated a liquid water mixing ratio parameterization (Hane and Ray 1985) using radar reflectivity at the lowest elevation angle. Bolton's (1980) approximation was used to compute θ_e. Further instrument specifications, including instrument errors and quality control techniques, are described by Straka et al. (1996) and Markowski et al. (2002).

To suppress small-scale noise, a filter was applied to the raw data. The filter used a triangular weighting function with a filter radius of 10-s. The exact scales retained by such filtering depend on vehicle speed, but generally, this filtering significantly damped features having spatial scales less than 200 m. Smoothed mobile mesonet observations were plotted in radar coordinates using time-to-space conversion. For the two cases examined here, the storm was assumed to remain relatively steady-state over the period in which the WSR-88D took one volume scan (5–6 min).

In order to make meaningful comparisons of FFDs from one case to another, it was useful to analyze deviations of θ_v and θ_e from a larger-scale "base state". The base states were dertermined by objectively analyzing meso-α-scale θ_v and θ_e values and interpolating the larger-scale θ_v and θ_e field to the loacation of the supercell.

WSR-88D data were used for both case days. Reflectivity factor at the lowest elevation angle was taken from the closest radar to the supercell. For the 16 May 1995 case, the Dodge City, Kansas WSR-88D (KDDC) was approximately 30 km south of the tornadic supercell, while on 20 May 1998, the Goodland, Kansas WSR-88D (KGLD) was approximately 80 km east of the nontornadic supercell.

3. Observations

a. 20 May 1998: Nontornadic supercell in eastern Colorado

On this day, conditions were conducive for supercell development in moist, upslope flow in eastern Colorado. East of the Laramie mountain range, a lee trough formed to the south of a stationary front. The supercell developed in Yuma county where it was sampled with the Goodland, Kansas WSR-88D.

Mobile mesonet observations in the FFD indicated θ_v deficits as large as 9 K (Fig. 2). Since θ_v included a reflectivity parameterization of liquid water, the field closely mimics the reflectivity pattern. Strong storm-relative winds advected slightly warmer air on the north side of the low-level circulation center, shown by the southwestward bulge of the -3 to -9 contours, while cold RFD air is rotating around the southern half of the mesocyclone.

Perturbation equivalent potential temperature, θ_e', is shown in Fig. 3 for the same analysis time. Deficits as large as 7 K are sampled in the FFD. Just to the northeast, close to the low-level circulation center, warm θ_e
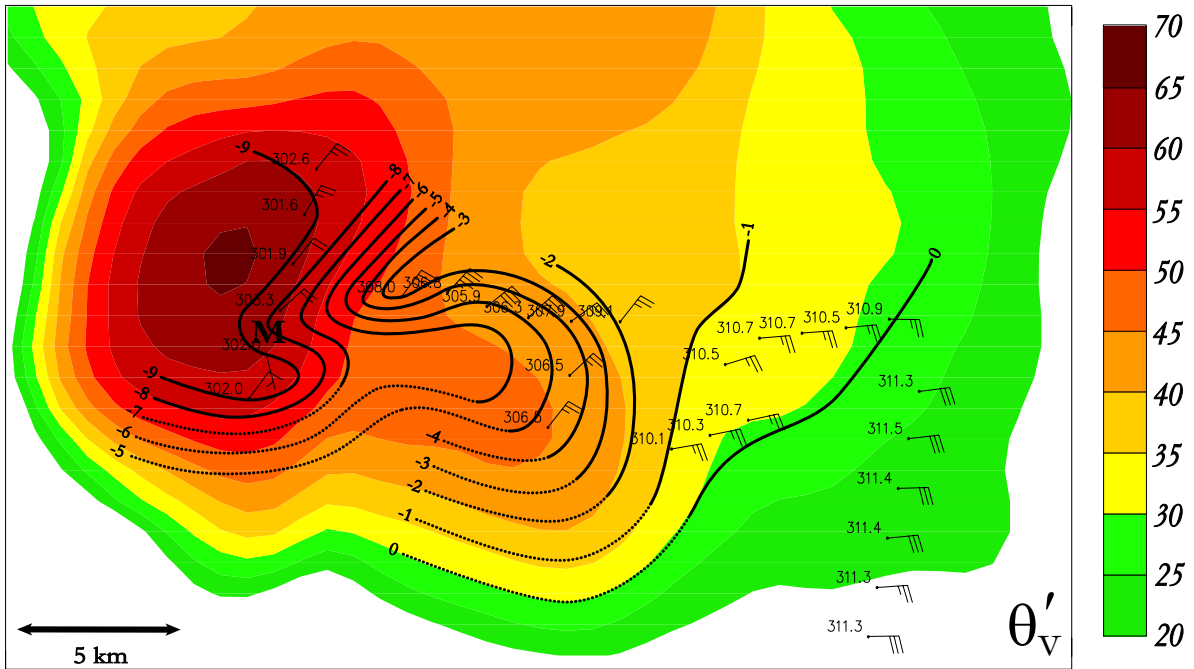
Fig. 2. Plot of perturbation virtual potential temperature, θ'_v (K, contoured), objectively analyzed reflectivity (shaded) and mobile mesonet observations at 01:15:58 UTC 20 May 1998. The contour interval is 1 K. Station models are plotted 1.5 km apart with storm relative winds depicted. A storm motion of $u = 8.41$ m s^{-1} and $v = 2.81$ m s^{-1} (from 200°) was calculated. Dotted contours reflect the lack of confidence owing to low observation density. The letter M denotes the low-level circulation center at the lowest elevation scan from the WSR-88D in Goodland, Kansas.
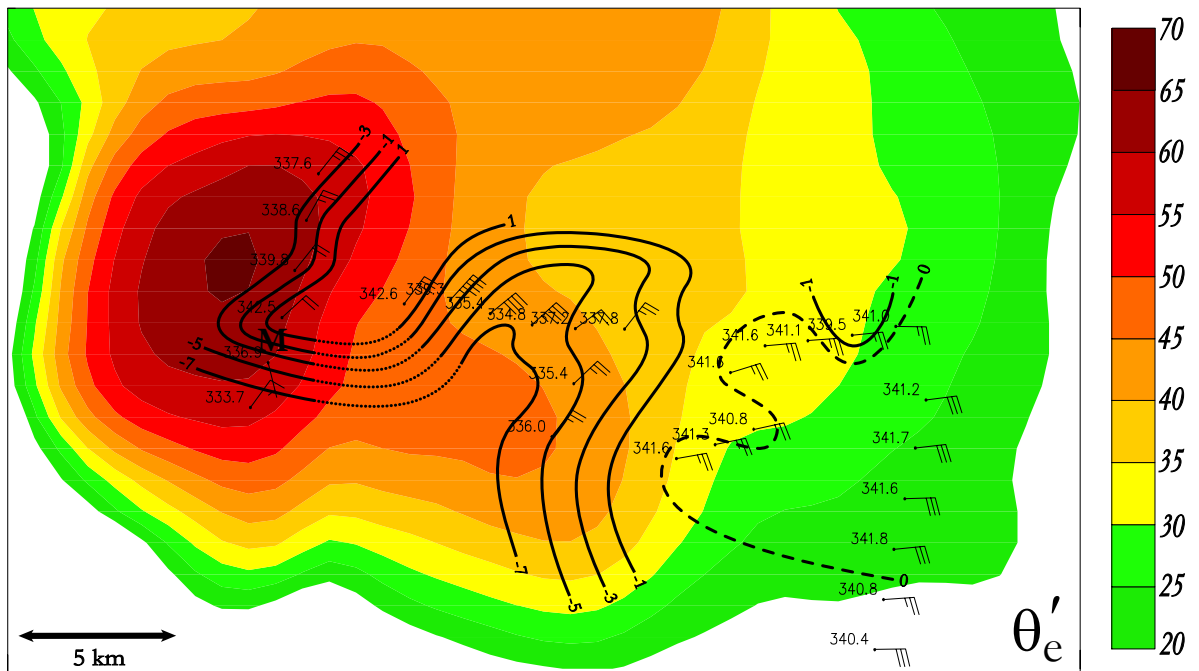
Fig. 3. As in Fig. 2 except perturbation equivalent potential temperature, θ'_e (K), is contoured. The contour interval is 2 K. The dashed line indicates an intermediate contour.

perturbations are shown which are converging into the low-level mesocyclone. The origin of the θ_e excesses is not known. Perhaps larger θ_e values were present aloft or perhaps the base state θ_e value was poorly specified.

b. 16 May 1995: Tornadic supercell in southwestern Kansas

A tornadic supercell was intercepted in southwestern Kansas near a triple point where a dry line and low pressure trough intersected. Several weak tornadoes and one strong tornado were observed between Jetmore and Hanston, KS between 2230 UTC and 0230 UTC.

The analysis of this storm is complicated by the fact that the storm was undergoing a discrete jump at this analysis time. The updraft to west was occluding and an eastward surging gust front initiated a new updraft base ahead of it. Larger gradients to the southwest of the new reflectivity maximum in both the θ_v' and θ_e' plots reveal the surge of the rear-flank gust front (Figs. 4 and 5). Difficulties defining the FFD region for this case arose owing to the presence of two updraft bases. However, closer examination of the radar data showed only one mesocyclone at low and midlevels associated with the initial updraft. In time, the new updraft forms along the initial updraft's forward-flank gust front and was included in the analysis.

Observations collected in and around the newly forming updraft, associated with the θ_e surplus, may not exhibit characteristics of rain-cooled FFD air, however, observations to the north of the new updraft possess more typical FFD characteristics reflected by the -1, -2 and -3 perturbation contours. Similar to Fig. 2, the θ_v' field is somewhat correlated with the reflectivity pattern (Fig. 4). The largest θ_v deficits sampled in the FFD were 3 K (Fig. 4), although slightly larger deficits were sampled in the RFD. The surplus of θ_e may have arisen from a mesoscale increase in base state θ_e that was not resolved by the synoptic observations and possibly led to a poor specification of the base state.

4. Summary and future work

Comparing and contrasting the analyses of the two supercell cases reveals differences between the θ_v' and θ_e' in each storm. In summary, analyses of these two cases indicate

- θ_v deficits in the FFD of the nontornadic case were 3–4 K larger than in the tornadic case

- θ_e deficits also were 3–4 K larger in the nontornadic case than in the tornadic case, with a similar finding of surface θ_e excess located near the updrafts in both cases

Future work will use similar data and analysis procedures on about a dozen case days roughly evenly divided between tornadic and nontornadic supercell cases. Once all cases are evaluated, it is our hope to have a clearer idea of the range of surface thermodynamic characteristics within FFDs and how these conditions are related to storm behavior and the large-scale environment.

REFERENCES

Bolton, D., 1980: The Computation of Equivalent Potential Temperature. *Mon. Wea. Rev.*, **108**, 1046–1053.

Brandes, H. E., 1984: Relationships Between Radar-Derived Thermodynamic Variables and Tornadogenesis. *Mon. Wea. Rev.*, **112**, 1033–1052.

Davies-Jones, R. P., and H. E. Brooks, 1993: Mesocyclogenesis from a theorectical perspective. *The Tornado: Its Structure, Dynamics, Prediction, and Hazards, Geophys. Monogr.*, No. 79, Amer. Geophys. Union, 105–114.

Doswell, C. A., and D. W. Burgess, 1993: Tornadoes and tornadic storms: A review of conceptual models. *The Tornado: Its Structure, Dynamics, Prediction, and Hazards, Geophys. Monogr.*, No. 79, Amer. Geophys. Union, 105–114.

Dowell, D. C., and H. B. Bluestein, 1997: The Arcadia, Oklahoma, storm of May 1981: Analysis of a supercell during tornadogenesis. *Mon. Wea. Rev.*, **125**, 2562–2582.

Hane, C. E., and P.S. Ray, 1985: Pressure and buoyancy fields derived from Doppler radar data in a tornadic thunderstorm. *J. Atmos. Sci.*, **42**, 18–35.

Klemp, J. B., 1985: Dynamics of tornadic thunderstorms. *Ann. Rev. Fluid Mech.*, **19**, 369–402.

———, and R. Rotunno, 1983: A study of the tornadic region within a supercell thunderstorm. *J. Atmos. Sci.*, **40**, 359–377.

Lemon, L. R., and C.A. Doswell III, 1979: Severe thunderstorm evolution and mesocyclone structure as related to tornadogenesis. *Mon. Wea. Rev.*, **107**, 1184–1197.

Markowski, P. M., 2002: Hook echoes and rear-flank downdrafts: A review. *Mon. Wea. Rev.*, **130**, 852–876.

Markowski, P. M., J. M. Straka, and E. N. Rasmussen, 2002: Direct surface thermodynamic measurements within the rear-flank downdrafts of nontornadic and tornadic supercells. *Mon. Wea. Rev.*, **130**, 1692–1721.

Rasmussen, E. N., and J. M. Straka, 1996: Mobile mesonet observations of tornadoes during VORTEX-95. Preprints, *18th Conf. on Severe Local Storms.* Amer. Meteor. Soc., San Francisco, 1–5.

Rasmussen, E. N., J. M. Straka, R. Davies-Jones, C. A. Doswell III, F. H. Carr, M. D. Eilts, and D. R. MacGorman, 1994: Verification of the origins of rotation in tornadoes experiment: VORTEX. *Bull. Amer. Meteor. Soc.*, **75**, 995–1006.

Rotunnno, R., and J. B. Klemp, 1985: On the rotation and propagation of simulated supercell thunderstorms. *J. Atmos. Sci.*, **42**, 271–292.

Straka, J. M., E. N. Rasmussen, and S. E. Fredrickson, 1996: A mobile mesonet for fine-scale meteorological observations. *J. Atmos. Oceanic Technol.*, **13**, 921–936.

Wakimoto, R. M., 2002: Convectively driven high wind events. *Severe Convective Storms, Meteor. Monogr.*, No. 50, Amer. Meteor. Soc., 255–298.

———, 1998: The Garden City, Kansas, storm during VORTEX 95. Part I: Overview of the storms life cycle and mesocyclogenesis. *Mon. Wea. Rev.*, **126**, 372–392.

———, L. Chinghwang, 1998: The Garden City, Kansas, storm during VORTEX 95. Part II: The wall cloud and tornado. *Mon. Wea. Rev.*, **126**, 393–408.

Walko, R. L., 1993: Tornado spin-up beneath a convective cell: Required basic structure of the near-field boundary layer winds. *The Tornado: Its Structure, Dynamics, Prediction, and Hazards, Geophys. Monogr.*, No. 79, Amer. Geophys. Union, 89–95.

Wicker, L. J., and R. B. Wilhemson, 1995: Simulation and analysis of tornado development and decay within a three-dimensional supercell thunderstorm. *J. Atmos. Sci.*, **52**, 2675–2703.

FIG. 4. As in Fig. 2 except the plot is valid at 01:00:15 UTC 17 May 1995. The storm motion calculated was $u = 11.36$ m s^{-1} and $v = 7.57$ m s^{-1} (from 215°). The contour interval is 0.5 K.

FIG. 5. As in Fig. 4 except perturbation equivalent potential temperature, θ'_e (K), is contoured. The contour interval is 2 K.